

Supporting Information

Swallowable Fluorometric Capsule for Wireless Triage of Gastrointestinal Bleeding

A. Nemiroski^a, M. Ryou^b, C.C. Thompson^b and R.M. Westervelt^{c,d}

^a Department of Chemistry and Chemical Biology, Harvard University, 12 Oxford St., Cambridge, MA 02138, USA.

^b Division of Gastroenterology, Brigham & Women's Hospital, 75 Francis Street, Boston, MA 02115, USA.

^c School of Engineering and Applied Sciences, Harvard University, 9 Oxford St., Cambridge, MA 02138, USA.

^d Department of Physics, Harvard University, 9 Oxford St., Cambridge, MA 02138, USA.

MATERIALS AND METHODS

General Circuit Design. Figure S1 shows a schematic of the circuit design. By using a system-on-chip (SoC) to integrate the microprocessor, radio, memory, and ADC, we have significantly reduced the overall circuit complexity and size of the device. The entire device platform can be divided into four distinct categories: i) the power supply (a battery and three separate voltage regulators to decouple the SoC, measurement, and LED driver circuitry); ii) the sense circuitry (photodiode, amplifiers, LED); iii) the SoC (which includes the microcontroller and radio); and iv) peripheral components (crystal oscillator, RF front-end, assorted passives).

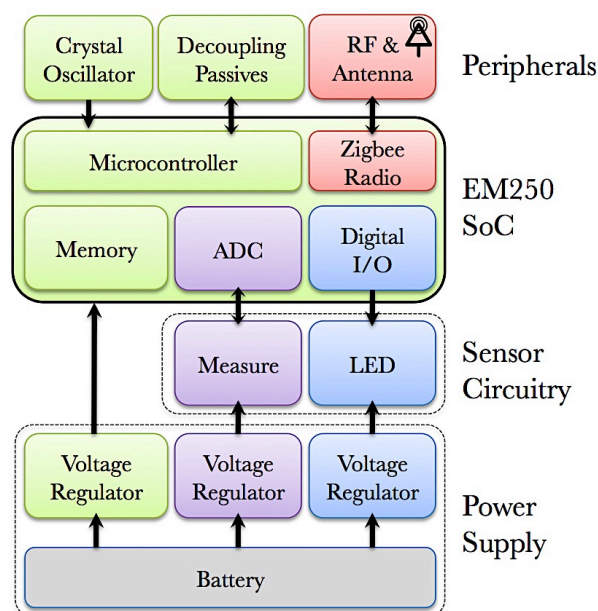


Figure S1. Block diagram of the hardware design. Blocks are physically grouped according to function. Color coding provides a guide to how subsystems interact.

Design of RF Stripline and Printed Circuit Board. Figure S2 shows a schematic cross-section of designs for the printed circuit board (PCB) and microstrip line. The PCB was designed to have four layers with a combined thickness of 0.031” and traces formed out of 1 oz copper. While the trace widths are not especially important for most of the signals and power routing, it was important to maintain a characteristic impedance $Z_0 = 50 \Omega$ for all traces in the RF circuitry. The characteristic impedance [1] for a microstrip line is defined by

$$Z_0 = \frac{87}{\sqrt{\epsilon+1.41}} \ln \left(\frac{5.98d}{0.8w+t} \right), \quad (S1)$$

where ϵ was the relative dielectric constant of the dielectric spacer layer, d the distance between the signal and ground layers, t the thickness of the signal trace, and w the width of the signal trace. Given that $\epsilon = 4.2$ for a 1080 dielectric (at 2.4 GHz), $d = 0.0057$ ” for the 4-layer PCB, and $t = 0.00141$ ” (1 oz copper), then to maintain $Z_0 = 50 \Omega$, the width must be $w = 0.009$ ”.

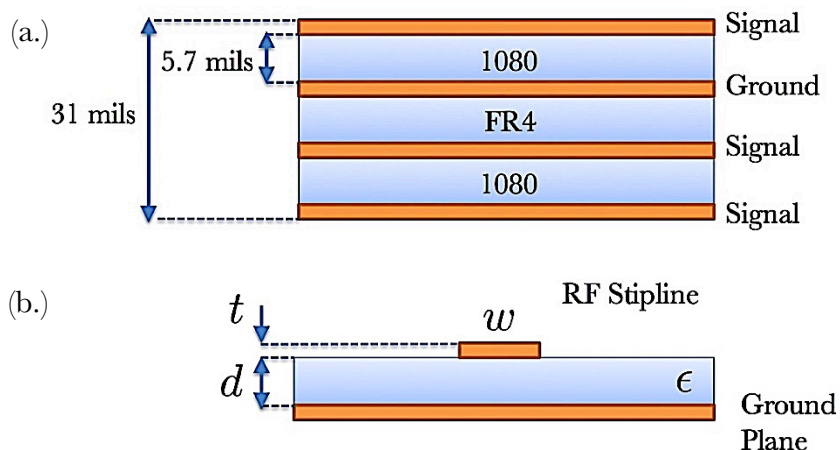


Figure S2. PCB Cross section. (a.) Cross section of 4-layer PCB. 1080 and FR4 are standard dielectric materials used in a PCB. (b.) Cross section of RF stripline.

Figure S3 shows the PCB layout for each layer. All components were placed as close as possible, with the minimum trace width and trace gap width of 0.007" (0.18 mm). The via holes all have an inner diameter of 0.008" and a total diameter of 0.018" (0.46 mm). Most passive components were in the 0402 package size ($0.4 \times 0.2 \text{ mm}^2$), which was the second smallest package size available for purchase through commercial vendors. The feedback resistor ($R_f = 500 \text{ M}\Omega$) for the TIA was in the 0805 package size ($0.8 \times 0.5 \text{ mm}^2$), and two inductors in the RF circuitry were in the 0603 package size ($0.6 \times 0.3 \text{ mm}^2$). The first (top) layer contains the EM250 SoC, measurement circuitry, voltage regulators, and entire RF front end, along with decoupling capacitors for the EM250. The second layer was designated as exclusively a ground layer. The third layer was for signal routing. The fourth (bottom) layer contains the crystal oscillator and associated passive components, the connection pads for the LED and photodiode from the fluorometer, and the current and voltage driving sources for the LED and measurement amplifiers.

Overview of Electronics Fabrication Process. The construction of the electronics was divided into four primary steps. i) Pre-cut the manufactured PCB to size. ii) Assemble all surface mount components and reflow solder paste. iii) Program microcontroller with custom firmware with a computer through a USB connection. iv) Finish cut the PCB to final size.

Cutting Out the Printed Circuit Board. Figure S4A shows the 4-layer PCB as manufactured by Advanced Circuits. Because design rules specified by the manufacturer impose a clearance of 0.04" between the edge of the cutout PCB and the nearest metal traces, the PCB needs to be cut to fit in the capsular form factor with a CNC mill. We chose to mill as much of the PCB as possible before surface mount assembly to reduce the chance of introducing cracks in the solder joints or components. To perform the cuts, the PCB was carefully mounted in a vice, and each cut made by a standard 1/8", 2-flute, square end mill. Figure S4B shows the milled PCB.

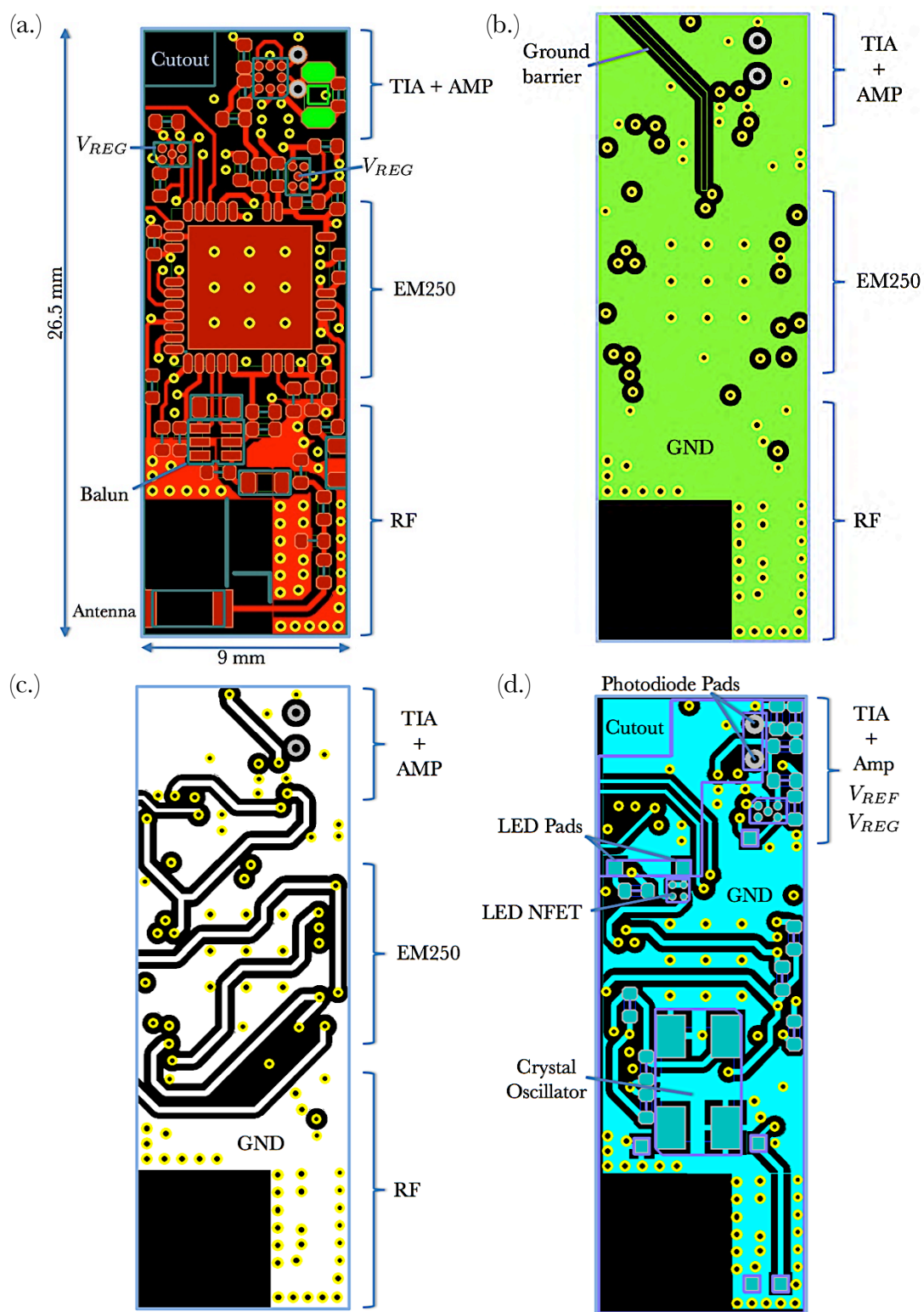


Figure S3. PCB layout. (a.) Top Layer. (b.) Ground layer. (c.) Signal Layer. (d.) Bottom Layer.

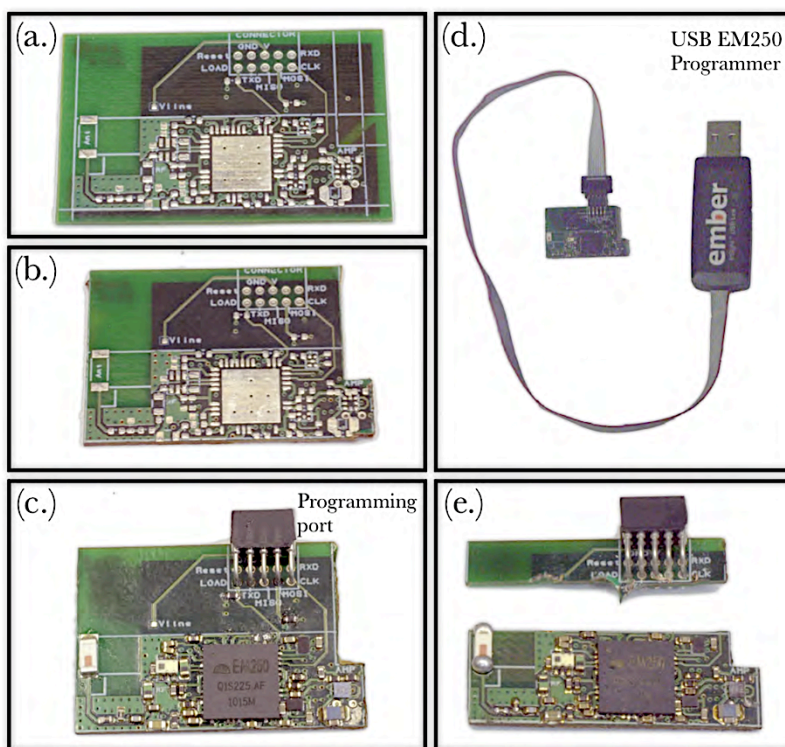


Figure S4: PCB fabrication process. (a.) PCB as supplied by the manufacturer. (b.) Pre-cut milling step. (c.) All surface mount components added to PCB and reflowed. (d.) USB programming connector attached to device. (e.) Final cut severs the programming connection and brings the PCB to its final size (9 mm x 26.5 mm).

Surface Mount Assembly. Assembly of the surface mount components was performed under a stereoscope. First, all pads on the topside of the PCB were coated with a liquid solder paste (Zephpaste SPE-0012, Zephyrtonics Inc.), applied with a needle. Next, each topside component was carefully placed with tweezers (*i.e.*, antenna, SoC, RF circuitry, voltage regulators, opamp package, and passive components). Although the voltage regulators and opamps have solder bumps on their pads applied by the manufacturer, we still applied solder paste to their PCB pads to aid in placement and adhesion. After placement, the pad alignment for each component was visually verified; minor misalignments were carefully corrected with tweezers. Once the topside was assembled, the PCB was placed in an infrared reflow oven (T-962, Taian Puhui Tech, CO, LTD.) to activate the solder flux, melt the solder, and permanently bond all the components. The reflow procedure lasted 5 minutes with a peak temperature of 250°C. Next, the bottom side of the PCB was assembled and reflowed by the same procedure as the topside. Solder bridges that shorted neighboring pads were mostly eliminated through the surface tension of the solder flux during reflow; any accidental solder-bridges that remained after reflow were manually repaired with a soldering iron.

Device Programming. To conserve space on the finished device, we designed the programming port to be permanently removed after the SoC was initially programmed. Figure S4C shows the 10-pin (5 pins x 2 rows) programming connector socket that was cut from a two row, 50 pin right angle socket (RT ANG 2X50 .050", Millmax, Inc.), and soldered into place. Figure S4D shows a proprietary programming cable (Insight USB Link, Ember Corp.) that connects the PCB to a computer through a USB connection to allow programming of the flash memory with custom firmware that we designed specifically for our application. The device firmware was written in the C programming language using a development environment and compiler (xIDE, Ember, Corp) specifically designed for the EM250 SoC. The development environment included all libraries and files unique to the Ember and Zigbee software stack. The device firmware for the capsular biosensor was based on the Sleepy-Sensor reference application supplied in the development kit (Ember, Corp.). The software was then compiled in xIDE and uploaded to the EM250 SoC via the USB cable by the communication software (Insight Desktop, Ember Corp.) supplied in the development kit.

Removal of Programming Port. Before the finishing cut was made, the crystal oscillator was removed using a heat gun, because we have found this to be the component most likely to be permanently damaged by the vibration caused by milling. Next, the PCB was mounted horizontally in a vise, and the port removed with a single, straight cut made with a standard 1/8", 2-flute, square end mill, at 1000 RPM. Figure S4E shows the PCB cut to final size along with the severed programming port. Finally, the crystal oscillator was soldered back into place, and the entire device reflowed one final time in the IR reflow oven (discussed in Section 7.3.3) to repair any cracks that may have developed in the hardened solder joints. We have found that ~80% of devices are fully functional after this entire PCB fabrication process; this value includes all attempts to fix initially unresponsive devices. The final PCB dimensions were 0.3543" x 0.6731" (9 mm x 26.5 mm), and the thickest points, including surface mount components, was 0.1" (2.54 mm) and occurred at the point where the EM250 SoC and crystal oscillator were aligned.

Fabrication of Optical Housing. Figure S5 shows CAD drawingS of the optical housing that we designed to hold together all the optical components of the fluorometer. We fabricated the housing by machining a 0.125" thick, black, Delrin acetyl thermoplastic sheet (DuPont, US) with a CNC mill. Figure S6A shows a schematic of how the filter slots were milled with a 0.02" diameter 2-flute square end mill (GR2SI 0.02, Roundtool Labs) at 2800 RPM, and the LED and photodiode slots were milled with a 0.04" diameter 2-flute square end mill (GR2SI 0.02, Roundtool Labs) at 2800 RPM. Next, the entire housing was cut out of the sheet with the 0.04" end mill. Figure S6B shows how, after the housing was cut out, we mounted it vertically drilled excitation pinholes with a 0.04" (size #60) micro drill bit and the emission pinholes with a 0.02" micro drill bit. Finally, a 0.02" thick housing cover was separately milled out from the same plastic following a similar procedure as the housing. Figure S6C shows an image of the fabricated optical housing. The cut overshoot seen in the all corners was an unavoidable product of cutting right angles with a round end mill. Figure S6D shows an image of the housing cover.

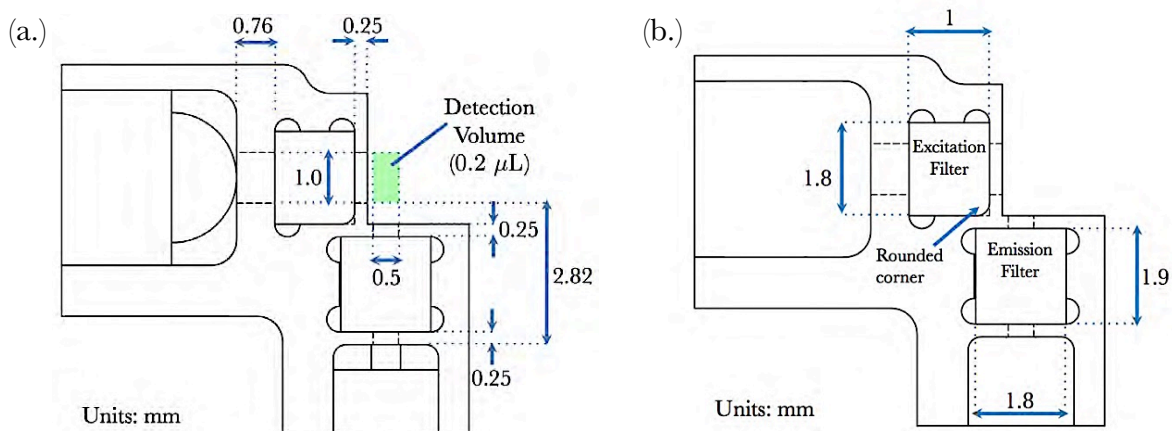


Figure S5: CAD Schematic of fluorometer optical housing.

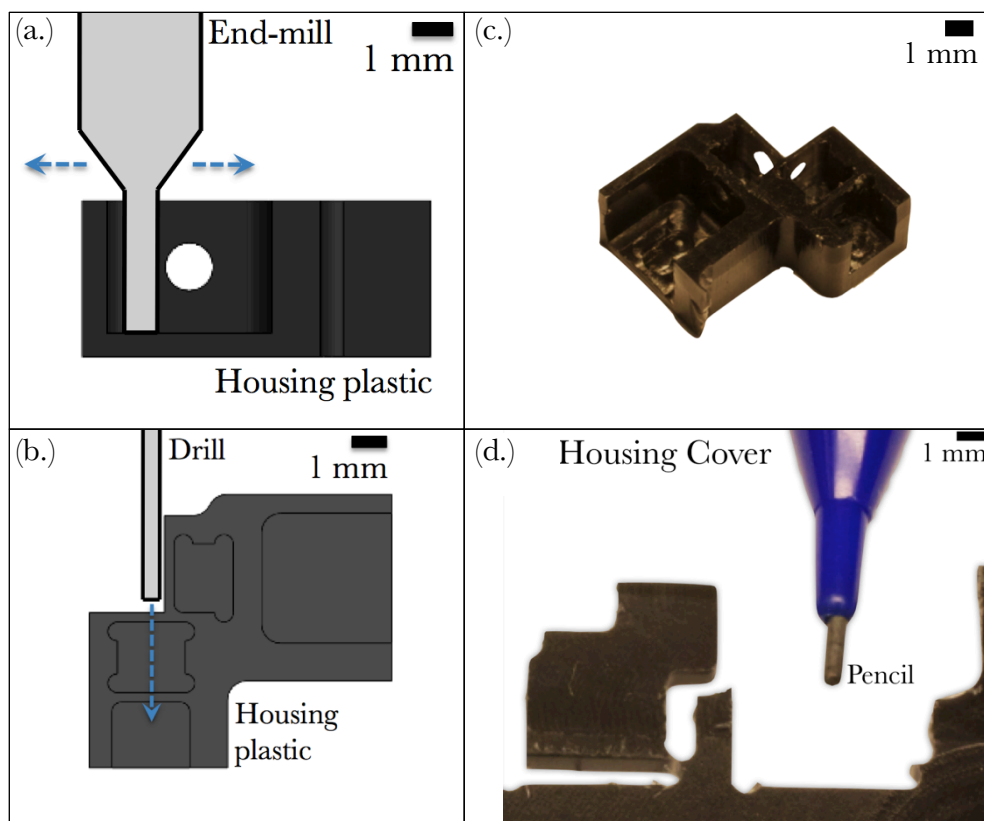


Figure S6: Fabrication of the optical housing and cover. (a.) Schematic detailing sequence for fabricating the housing with a CNC mill. (b.) Schematic detailing sequence for drilling pinholes. (c.) Finished optical housing. (d.) Housing cover shown attached to the plastic sheet after milling (connection is severed when the cover piece is needed).

Dicing the Optical Filters. The fluorometer has two optical filters: a low pass excitation filter (NT64-593, Edmund Optics) and a bandpass emission filter (MF525-39, Thorlabs). To fit into the miniature fluorometer, the filters needed be cut into small squares. Figures S7–S8 show the dicing procedure for cutting the filters. First each large filter was mounted on a silicon wafer with melted wax using a hotplate (Fig. S7A and S8A). Next, the wafer with mounted filters was diced with an automatic diamond saw (DISCO DAD-321) into $1.8 \times 1.8 \text{ mm}^2$ squares to fit into the optical housing (Fig. S7B and S8B). After dicing, the wax was re-melted using a hot plate so that the filters can be removed from the wafer. Because dicing saw can only cut 1.5 mm deep, the excitation filter could be diced all the way but the emission filter could not. The excitation filter squares, therefore, can be individually removed from the wafer but the emission filter was removed as a solid piece (Fig. S8B). The cuts in the emission filter, however, were deep enough such that it can be carefully broken apart into its constituent filter squares (Fig. S8C). A single corner of each excitation filter square was then rounded off with a diamond wheel saw (Model 650, South Bay Technology, Inc.) to fit into the optical housing. The edge of each square of the emission was planarized with a grinding wheel to eliminate jagged features incurred while breaking each filter off. Finally, each filter square was individually cleaned of wax and debris with a swab soaked in methanol. A single 12.5 mm diameter excitation filter yielded 25 squares, and a single 25 mm diameter emission filter yielded 60 filter squares.

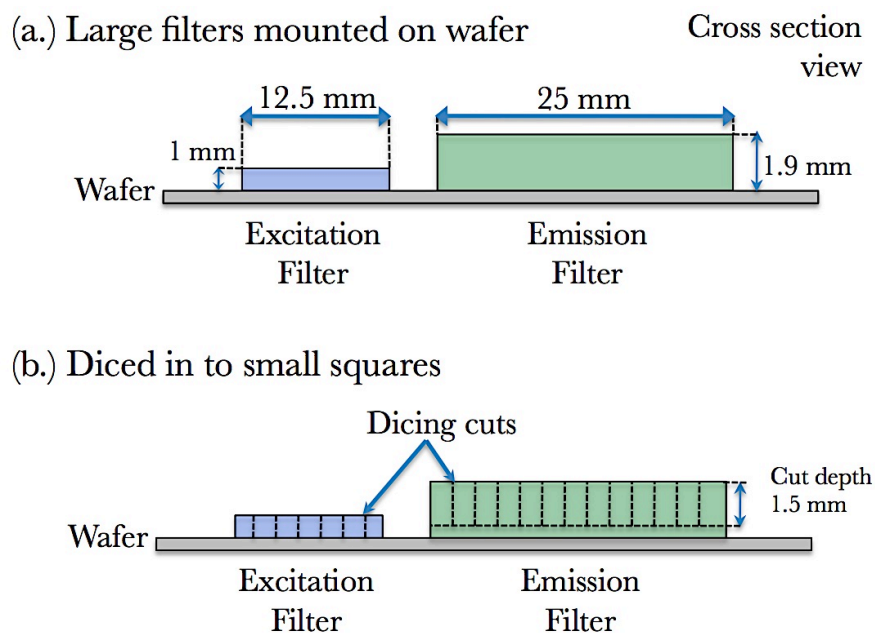


Figure S7: Schematic depicting cutting of filters. (a.) Large filters are mounted on a silicon wafer with melted wax. (b.) Filters are diced in small squares by a wafer-dicing saw with a cut depth of 1.5 mm.

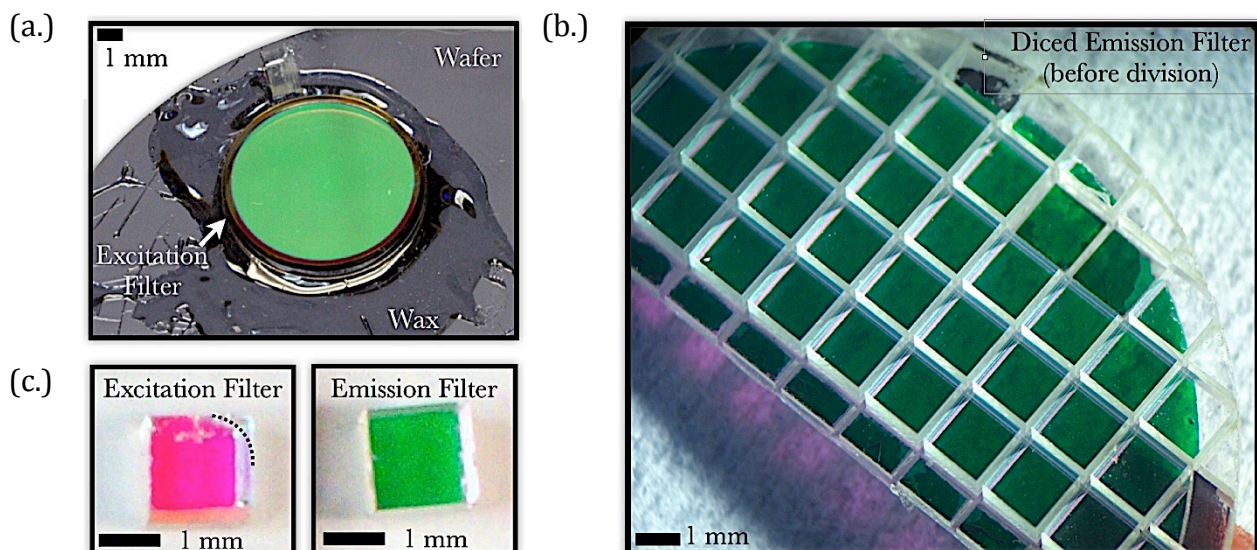


Figure S8: Fabrication of Filters. (a.) Emission filter mounted on silicon with wax. (b.) Excitation filter after dicing with a 1.5 mm cut depth. (c.) Excitation and emission filter squares after dicing. Emission filter is manually broken apart to form the squares. A corner of the excitation filter is rounded off with a diamond-coated grinding wheel to fit the optical housing (indicated by curved dotted line in figure).

Fluorometer Assembly. The fluorometer was assembled out of i) a photodiode (PDB-C122, Advanced Photonix, Inc.); ii) an LED (LB E63C, OSRAM, Inc.); iii) diced excitation and emission filters; and iv) a milled plastic housing and cover. First, the LED and photodiode were inserted into their respective slots. These two components were fixed in place with a 2-part optically clear epoxy (Bondit-45, Reltek), which was specified for bonding difficult to bond plastics such as Delrin. Before inserting the optical filters, their perimeters were first coated in a thin layer the epoxy to prevent fluid from leaking in through the pinholes. Next, the optical filters were inserted into their respective slots. The epoxy coated the entire filter slot interior, while surface tension prevents it from filling in the pinhole area. Finally, the housing cover was bonded to the housing with a thin layer of epoxy. The epoxy remained in a liquid form throughout the entire assembly process (30 min.). Finally, the entire fluorometer was baked in air on a hot plate at 90°C for 3 hours to cure the epoxy. Figure S9 shows an image of the finished fluorometer assembly. Figure S9B shows the active area of the photodiode as seen through the emission filter pinhole to confirm that it was well aligned with the pinhole.

Mounting of the Optical Housing. The housing cover of the assembled fluorometer was first coated with a thin layer of epoxy. Next, the fluorometer was mounted on the backside of the PCB, and aligned with the right-angle PCB cut. The device was placed on a hot plate and baked in air at 90°C for 3 hours to cure the epoxy. Next, the LED and photodiode were connected to the PCB by manually soldering a short piece of wire between the component pads (two per component) and their corresponding PCB pads. Figure S10 shows the mounted optical housing and manually soldered connections.

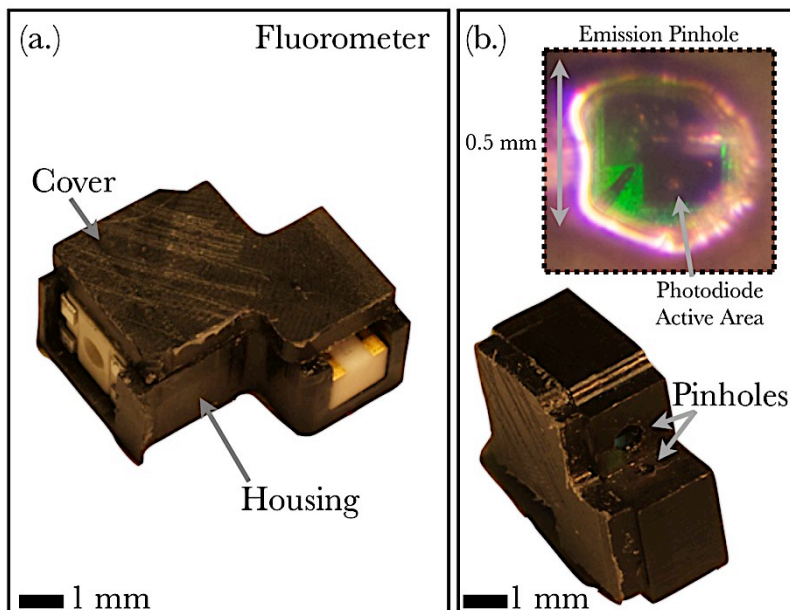


Figure S9: (a.) Fully assembled fluorometer. (b.) Different view of the fluorometer. (Inset) A view through the emission pinhole to reveal the proper alignment of the photodiode active area.

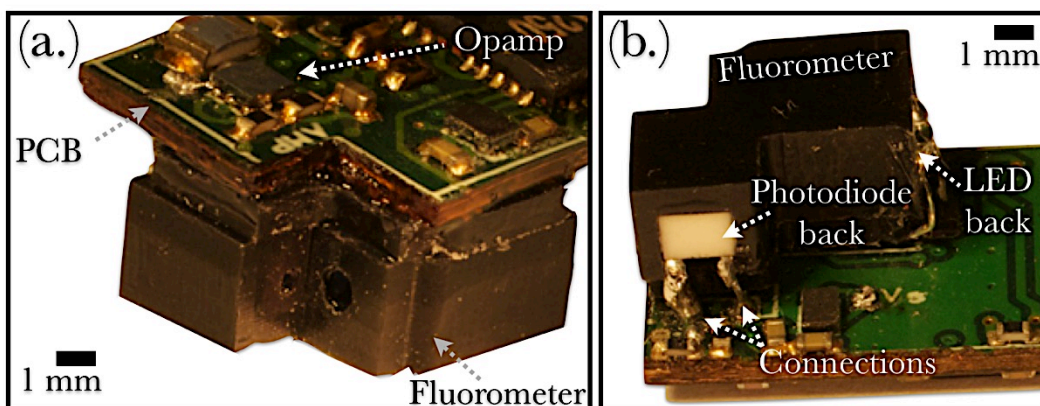


Figure S10: (a.) Fluorometer mounted to the PCB with epoxy. (b.) Electrical connections made between the LED, photodiode, and corresponding PCB pads.

Mounting of the Battery. A miniature re-chargeable lithium-polymer battery (LP30-FR, Plantraco, Inc.) was mounted with Super Glue (Super Glue Corp.) to the back of the PCB, directly onto the crystal oscillator. A wire was manually soldered to make a connection between the V_{BATT} pad of the PCB and the positive terminal $V+$ of the battery. Separate wires were also manually soldered to the PCBs ground pad V_{GND} , and to the positive $V+$ and negative pins $V-$ of the battery. The battery was charged by connecting these extra $V+$ and $V-$ wires to a battery charger (Plantraco, Inc.) specifically designed for use with this battery. When the battery was fully charged, a solder connection was made between the V_{GND} and $V-$ to activate the battery and turn on the device. Figure S11A shows these connections.

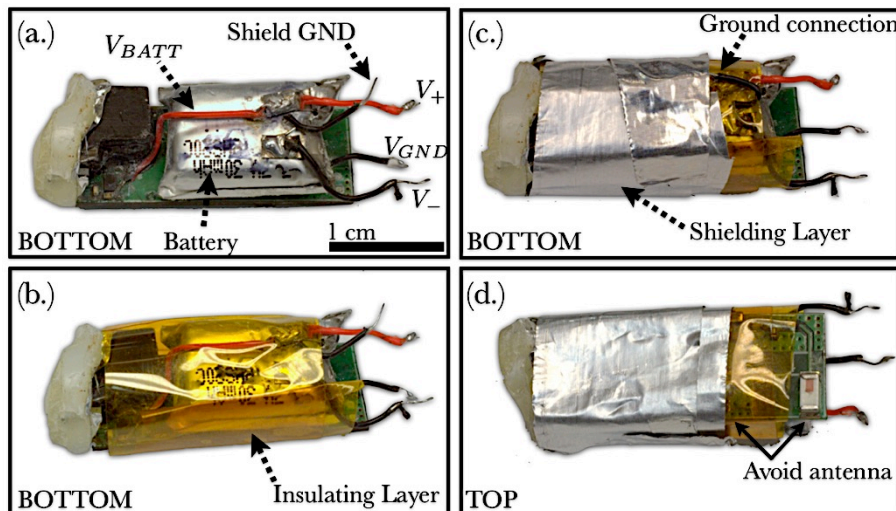


Figure S11: (a.) Battery is glued to the bottom side of the PCB and wires attached. (b.) Device is wrapped in an insulating layer of Kapton tape. (c.) Device is wrapped in a conductive shielding layer of aluminum foil and grounded through a wire to the battery's negative terminal. (d.) Top view of the shielded device, revealing the exposed antenna.

Device Shielding. The device was wrapped with an insulating layer of Kapton tape (Figure S11B) and then wrapped with aluminum foil (Figure S11C) to provide a conductive shielding layer that prevents electronic interference from external sources that can introduce noise into the measurements. The shielding layer was secured and grounded by fixing one of the extra V- wires to the aluminum foil with a conductive tape. Figure S11D shows how the shielding layer was wrapped in a way as to avoid any overlap with the antenna to ensure high quality performance of the RF communication.

Capsular Packaging. A cylindrical capsule was fabricated out of a white plastic rod (Delrin acetel thermoplastic; Dupont, US). The rod was mounted in a lathe, and a 0.413" (10.5 mm) inner diameter (ID) was drilled and reamed at 1300 RPM. Next, the outer diameter (OD) was carved down to 0.433" (11 mm), forming a wall thickness of .01" (0.25 mm), and 1.043" (26.5 mm) of the capsule sliced off: these form the final dimensions of the capsule. Finally, the capsule was mounted onto a complementary plastic rod with OD 0.413" and clamped in a vice. A corner was milled out to match the geometry of the fluorometer and PCB. The capsular end cap was fabricated with the same process, except the ID drilling/reaming step was altered to ensure a depth of 0.65" (16.5 mm). The capsular end cap was then sliced off 0.02" (0.5 mm) past the drilled/reamed depth to form a final length of 0.67" (17 mm), and a 0.02" base. The PCB with fluorometer and battery was inserted into the capsule and the fluorometer end closed off with epoxy to provide a watertight seal. The device was again heated on a hotplate at 90°C for 3 hours to cure the epoxy. Figure S12A shows how the capsule was next wrapped in Teflon tape to make a watertight seal with the end-cap and Figure S12C shows how the capsule and end-cap were joined together. The final device had a diameter x length of 11 mm x 27 mm.

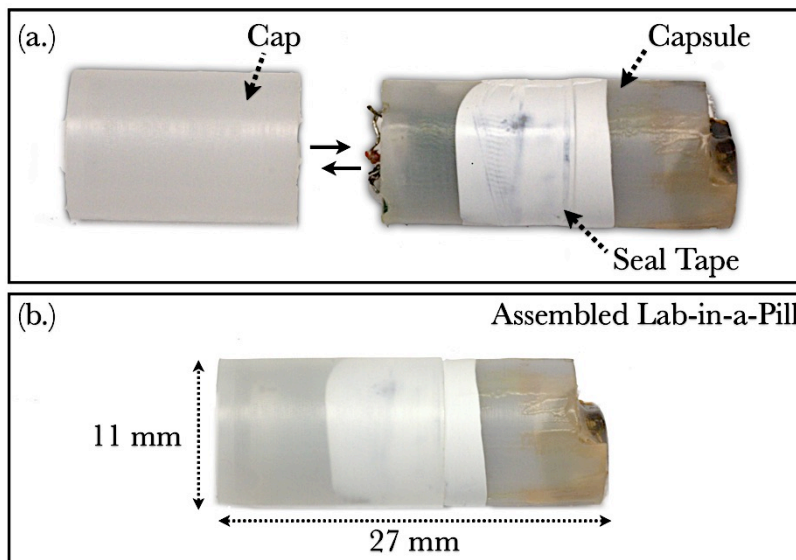


Figure S12: Final device assembly. (a.) PCB inserted into capsule and sealed with epoxy. Teflon seal tape is then wrapped at the end-cap connection point. (b.) End cap and capsule joined together.

Workflow of Software and Data Acquisition. Figure S13 shows the workflow for the custom software that we developed for the microcontroller to control the swallowable biosensor and to direct the flow of information between data acquisition to wireless communication. This basic structure is compatible with any microcontroller that has an ADC and the capability to control a Zigbee radio. After uploaded the software to the device and powering it on, the device ran subroutines that initialized the hardware and Zigbee stack. Then, the device sent a sequence of messages to find a parent node and continued doing so until it found a parent device. Once it successfully joined the network, the device began an internal timer that dictated how often to take a measurement. If it was not yet time to take a measurement, the device went into a low power sleep mode. According to the Zigbee protocol, for a sleeping device to remain on the network, it must periodically wake up and send a brief message to confirm that it is still operational; this sequence is to as “polling” the network. Polling enables an external monitor device to always know if the capsular biosensor is functional, regardless of the outcome of a measurement. Every time the device wakes up the poll the network it checks whether it is time to acquire a measurement yet.

If it is time to acquire data, the device proceeds according to the workflow shown in Figure S13. The data acquisition sequence uses a logic signal to pulse the LED on and off N_{LED} times with a 50% duty cycle for a total time Δt_{PULSE} . During each cycle the device acquires voltage measurements continuously, at a sampling rate imposed by the specific choice for ADC. Finally after all the data is collected, it numerically multiplies the data by a square wave with the same frequency and phase as the LED pulses and averages all the points together. This is the digital “lock-in” filtering used to both narrow the measurement bandwidth to reduce noise, and extract the modulated signal so that it can be represented by a single number, the amplitude of the

signal. Finally, once the data is acquired, the single data value is sent to the external monitor by a single Zigbee data packet. The external monitor is then free to forward the data through the hospital network to the medical personal monitoring the patient. Following the transmission of data, the device immediately powers down into its low power sleep mode. After a pre-determined time, it wakes up to poll the network, and continues this sequence again.

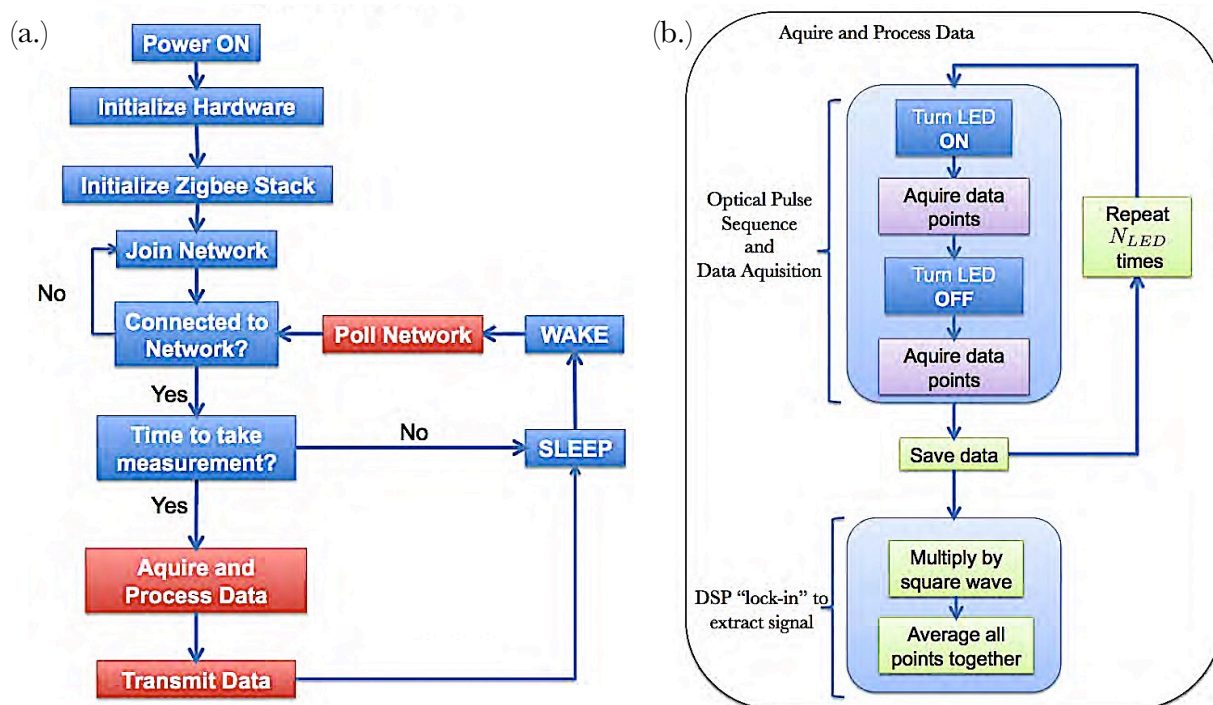


Figure S5: Software workflow of swallowable biosensor. Software data acquisition sequence.

EXPERIMENTAL DESIGN

Optical Characterization of Filters. Figure S14 shows the overall experimental setup that we used to optically characterize the optical components of the fluorometer. The transmission spectra of the filter optics were collected by partially assembling a fluorometer that only contained optical filters (without the LED or photodiode). The fluorometer was then fixed with a clamp, and exposed to a white light source (100 W Mercury lamp, Chiu Tech. Corp.). The output spectrum was collected by a step-index multimode optical fiber (1 mm core; BFH37-1000; Thorlabs, Inc.) and measured by a spectrometer (HR2000CG-UV-NIR; Ocean Optics, Inc.), which output data through a USB connection to a personal computer. The acquired spectral data was analyzed in SpectraSuite (Ocean Optics, Inc.). The reference spectrum of the white light source was first measured by exposing the fiber aperture directly to the light source. Figures S15a–b show, in detail, how we arranged the components to collect the spectrum of each

individual filter. In each case, we inserted the optical housing into the optical path without disturbing the light source or fiber. We used a clamp to fix the fluorometer such that each filter was alternately aligned with the white light source and the collection fiber, for each optical filter. The filter transmission was calculated by subtracting the reference spectrum from the filter output spectrum.

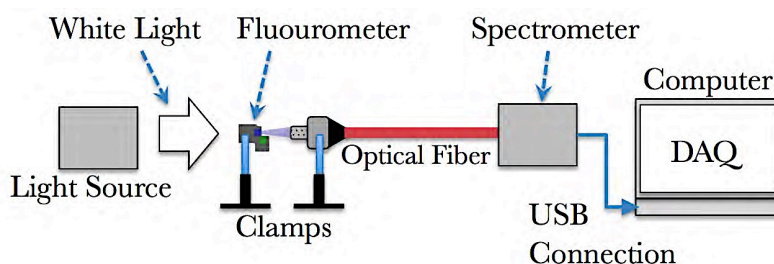


Figure S14: Measurement set-up for characterizing optical transmission spectra.

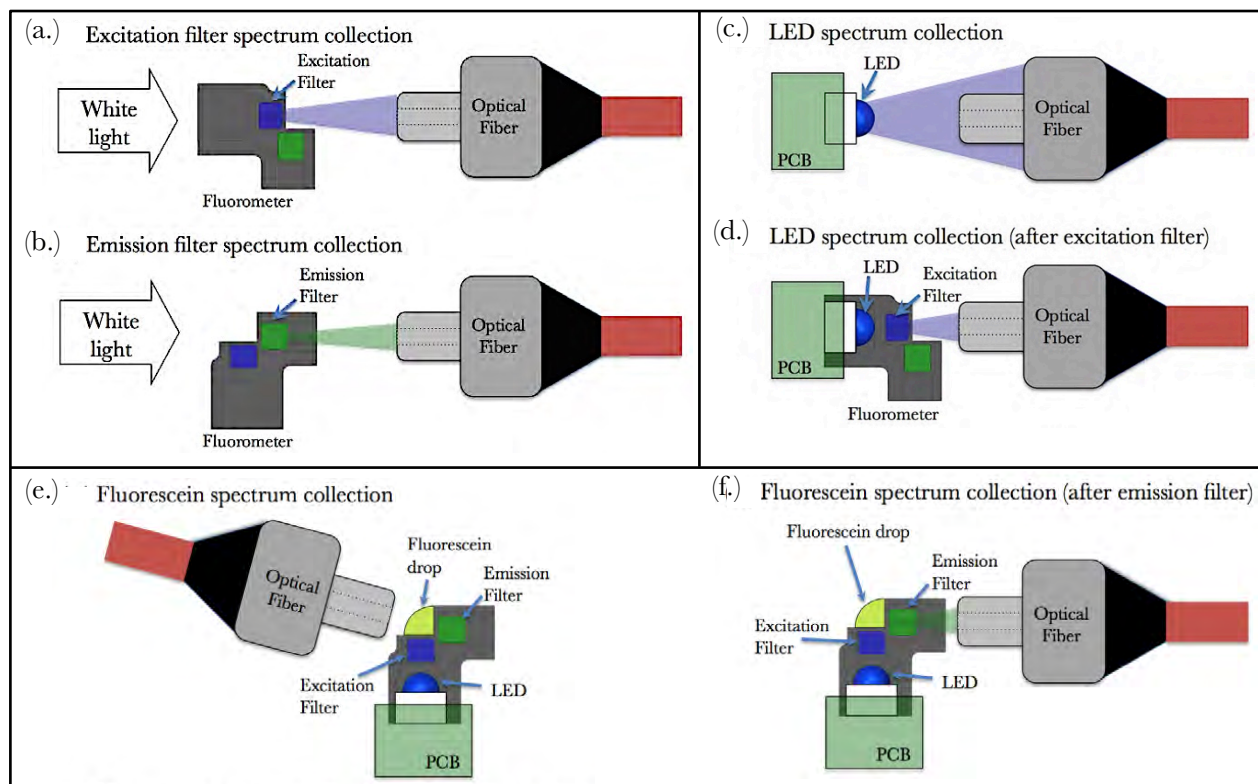


Figure S15: Experimental set-up for collection of transmission spectra through the excitation filter (a.) and emission filter (b.). Experimental set-up for collection of optical spectrum from the (c.) LED and (d.) LED light transmitted through the excitation filter.

Optical Characterization of LED and Fluorescein Emission. Figure S15c shows how we collected the raw spectrum of the LED. The LED was soldered to a small PCB and then connected to a 3.3 V power supply that sourced the 10 mA current needed to drive the LED. We then inserted the LED (on PCB) into the optical housing. Figure S15d shows how we collected the spectrum of the LED after transmission through the excitation filter. The fluorometer (with LED and excitation filter) was inserted into the optical path without disturbing components and then we collected the LED spectrum that was transmitted through the emission filter.

Figure S15d shows how we collected the emission spectrum of fluorescein by mounting the fluorometer vertically with a clamp, while the LED was attached to the PCB. A droplet of deionized water with a concentration $C = 10 \mu\text{M}$ of dissolved fluorescein was placed into the detection volume and stabilized by surface tension. The LED was then activated and the emission spectrum of the fluorescein recorded. Figure S15f shows how we collected the spectrum of the fluorescent emission that reaches the photodiode. So that relative intensities can be compared, we maintained an equivalent solid angle by maintaining a constant distance between the fiber apertures to the detection volume.

We measured the angular spectrum of the emission filter to gauge the effectiveness of the pinholes. We first measured the reference spectrum of the halogen lamp, and then mounted an uncut emission filter into the optical path with a standard 25-mm filter mount. Figure S16 shows how we collected the spectrum transmitted through the filter with an optical fiber. By rotating the filter, we collected the spectrum at $\theta = 0^\circ$ and at $\theta = 17^\circ$, which corresponded to the maximum acceptance angle enforced by geometry of the emission pinholes, which were 0.5 mm in diameter and were spaced apart by 1.9 mm. Figure 6B in the main text shows these data overlaid on one plot. In this figure, the LED and fluorescein spectra were normalized to their corresponding unfiltered spectra. Figure S17 shows a plot of all the spectra that we collected.

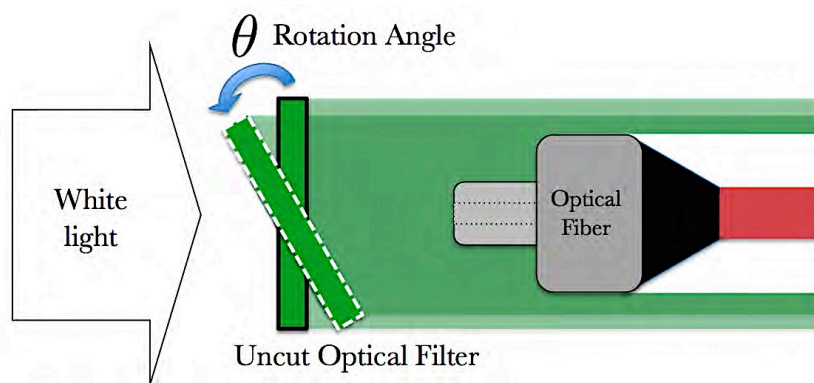


Figure S16: Measurement set-up for collecting the angular spectrum of an uncut excitation filter.

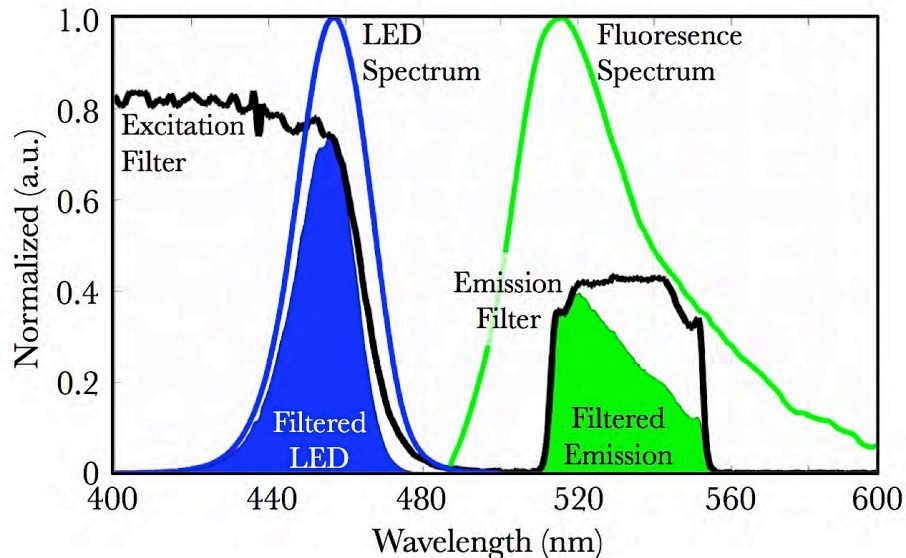


Figure S17: Optical transmission spectra of the excitation filter and emission filter, filtered and unfiltered LED excitation spectrum, and filtered and unfiltered fluorescein emission spectrum.

Configuration of USB dongle as parent node. We used a single wireless Zigbee transceiver in the form of a USB dongle (ETRX2; Telegesis, Inc) as the external monitor (parent device) to stream data wirelessly to a personal computer from the capsular biosensor. The proprietary USB stick contained the same EM250 SoC as the capsular biosensor device that we developed, and was programmed over a virtual serial interface through the USB port with custom firmware written in C using the xIDE development environment (Ember, Corp.) and uploaded through InSight Desktop (Ember, Corp.). As soon as the USB monitor device was plugged into a personal computer, and the capsular device turned on, they both announced their roles in the Zigbee network by exchanging corresponding Zigbee packets; this process was completely automated through the Zigbee stack libraries supplied by Ember for use with the EM250, and is part of the firmware uploaded to both devices. Once the MAC address of the capsular device as recognized (we hardcoded the address into the software of the USB monitor), the capsular device automatically began to stream data wirelessly through the Zigbee RF connection. Any further updates to the software of the capsular biosensor could be performed wirelessly “over-the-air” with InSight Desktop together with the USB monitor. The initial firmware upload, however, was made through the wired connection—before the programming port as permanently removed from the PCB of the capsular device—because the firmware libraries enabling over-the-air updating are not preloaded on the EM250 out of the box.

Setup for Performing Noise Measurements with the Capsular Device. Figure S18 shows the measurement setup that we used for capturing all data with the capsular device. Once the capsular device and USB monitor were activated, they automatically formed a wireless connection. Using software for data acquisition written in MATLAB (Mathworks, Inc.) we

established communication with the USB monitor through a virtual serial port interface. Each data point transmitted by the capsular sensor was sent to MATLAB software through the USB monitor and recorded. The capsular device was placed on a wooden table 1 m away from the USB monitor and continuously streamed acquired data. Since fluorometer is sensitive to white light from the room lights and computer monitor, we therefore placed a small cardboard box over the device and turned the room lights off, to simulate the darkness encountered within the GI tract.

Setup for Acquiring Fluorometric Measurements. Figure S19 shows measurement setup for acquiring fluorometric measurements. We filled a small beaker with 200 mL of de-ionized water and submerged a small magnetic stirring rod (VWR, Inc.) at the bottom. The capsular biosensor was lowered into the beaker and fixed in place with a clamp, approximately at the center of the beaker. The entire setup is placed on a magnetic stirrer (Thermolyne, Inc.) and stirred at 600 RPM throughout the experiment to aid in rapid mixing and to simulate the churning of the stomach and movement of the patient.

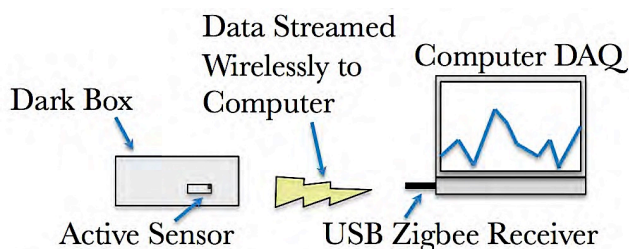


Figure S18: Measurement set-up for acquiring wireless data from the capsular device for characterization of noise performance.

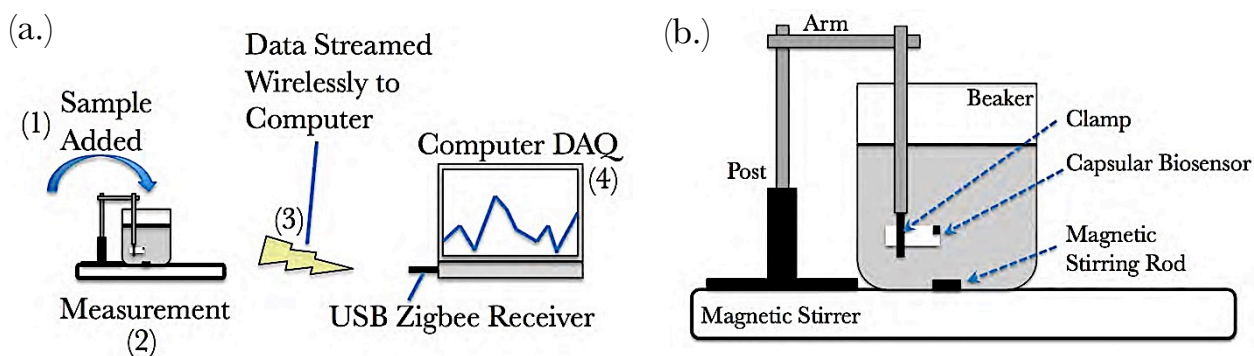


Figure S19: Set-up for wireless optical measurements used to collect the data presented in Figure 7 (main text). (a.) The overall setup; the parenthetical numbers indicate the sequence of events during a measurement. (b) Close-up of the measurement stage.

RESULTS

Measurement of electronic noise before digital filtering. The MATLAB DAQ program first sent a command to the capsular device to disable the LED and DSP filter so that the raw dark noise data could be streamed to the computer exactly as input to the ADC. The ADC then sampled $N = 18$ points of data at $f_S = 1.65$ kHz during each DAQ cycle, which we set for a duty cycle of 3 s. Every time a new cycle was executed and received by the computer, it was concatenated with all previous raw data. Finally, after $L = 7002$ total data points (389 consecutive DAQ cycles) were collected, we performed an L -point discrete Fourier Transform (dFT) on the acquired data. The resolution of the frequency bins of the dFT resolution bandwidth was $\Delta f_{RBW} = f_S / L = 0.236$ Hz. With the low-frequency gain H of the analog front-end (TIA followed by 50x amplification stage) fixed at $H = 16.5$ mV/pA, then the measured, input referred current noise spectral density i_{exp} is defined Equation S2.

$$i_{exp} = \text{dFT}[\text{Raw Data}] \cdot \sqrt{\frac{2}{L \cdot \Delta f_{RBW}}} \cdot \frac{1}{H} \quad (\text{S2})$$

The second term in Eq. S2 scales the raw dFT (first term) to a 1 Hz bandwidth. The factor of $\sqrt{2}$ combines the positive and negative amplitude spectrum into a single positive spectrum. The final term in Eq. S2 reverts the output-referred spectrum of the voltage noise (as sampled by the ADC) to the spectrum of the input-referred current noise. Figure S20 shows i_{exp} , along with theoretical input-referred current noise spectral density i_{th} calculated by assuming that all resistors (including the impedance of the photodiode and input impedance of the opamps) produce Johnson-Nyquist noise and all current sources (opamp leakage current and photodiode dark current) produce shot noise. (For an excellent reference on TIA noise calculations, see Graeme, 1996 [2]). To compare i_{exp} and i_{th} , we include the result of a 50-point moving average (smoothing) filter performed on i_{exp} . We found that in a flat region around $f = 10$ Hz within a 10 Hz bandwidth (indicated by the green box in Fig. S20), the average noise spectral densities of the measured vs. theoretical values were in close agreement ($\langle i_{exp} \rangle = 9.35$ fA/ $\sqrt{\text{Hz}}$ and $\langle i_{th} \rangle = 9.33$ fA/ $\sqrt{\text{Hz}}$). The total standard deviation of the unfiltered data was found to be $\sigma^{(I)} = 176.7$ fA.

Measurement of electronic noise after digital filtering. We sent a wireless command through the USB monitor to the capsular device to activate the digital filter, which performed a 40 cycle “lock-in” type filter on the sampled data of 18 points per cycle to collect a total of $N = 720$ points per DAQ period and reduce the measurement bandwidth to 1.15 Hz. The capsular device then collapsed these N data points into a single average value, which it transmitted to the USB monitor once every 3 s. Figure S21 shows a comparison between the filtered data (after 200 DAQ periods) and the unfiltered data (collected in the previously). By imposing the digital averaging filter, we were able to reduce standard deviation of the acquired data down to $\sigma^{(N)} = 10.2$ fA. This result corresponds well with the theoretically expected result 10.1 fA, which can be found by substitution into Equation S3, and indicates the digital filter works as designed.

$$\sigma^{(N)} = \sigma^{(1)} \sqrt{\frac{f_n/f_e}{N}} \quad (\text{S3})$$

In Eq. S3, $f_n = f_s / 2 = 825$ Hz is the Nyquist window of the ADC and $f_e = 350$ Hz is the effective bandwidth of i_{exp} . The quantity f_e is the frequency at which a hypothetical, rectangular spectrum—with height matched to the low frequency gain of the original spectrum (in this case, ~ 10 fA/ $\sqrt{\text{Hz}}$)—must cutoff to maintain the same total integrated noise power as the original spectrum. The limit-of-detection (LOD) of input-referred current is thus $I_{LOD} = 3\sigma^{(N)} = 30.6$ fA.

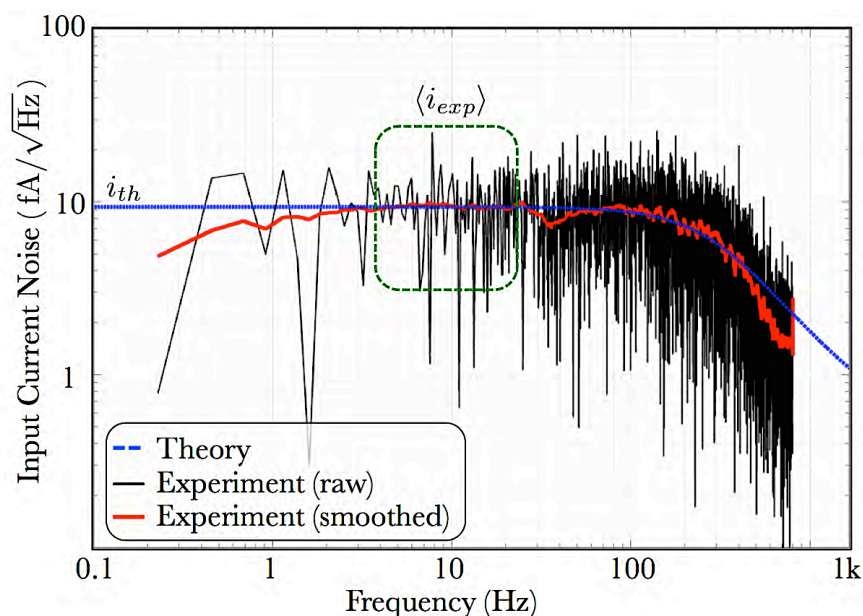


Figure S20: Experimental and theoretical input referred current noise. A 50-point smoothed version of the experimental data is shown in red.

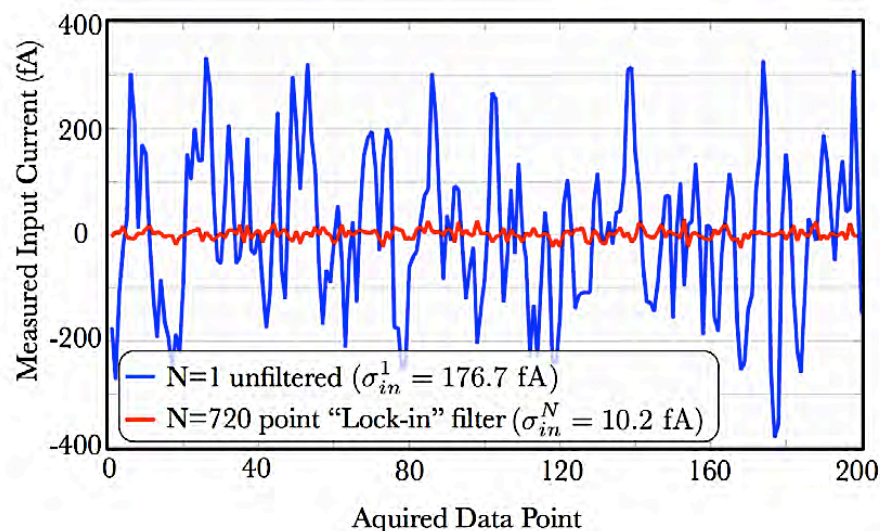


Figure S21: Time trace of unfiltered, raw data (blue) and data filtered digitally by the capsular device ($N = 720$ points, 40 cycle “lock-in” filter, 1.15-Hz bandwidth).

REFERENCES

- [1] Wheeler, Harold A. "Transmission-line properties of a strip on a dielectric sheet on a plane." *IEEE Transactions on Microwave Theory and Techniques*, 1977, **25** (8), 631-647.
- [2] J. G. Graeme, *Photodiode Amplifiers: OP AMP Solutions*. McGraw Hill Professional, 1996.